

Article pubs.acs.org/JACS

Bimolecular Reductive Elimination of Ethane from Pyridine(diimine) Iron Methyl Complexes: Mechanism, Electronic Structure, and Entry into [2+2] Cycloaddition Catalysis

Carli B. Kovel, Jonathan M. Darmon, S. Chantal E. Stieber, Gisselle Pombar, Tyler P. Pabst, Bastian Theis, Zoë R. Turner, Okten Ungör, Michael Shatruk, Serena DeBeer, and Paul J. Chirik*



Cite This: J. Am. Chem. Soc. 2023, 145, 5061-5073



ACCESS I

III Metrics & More

Article Recommendations

Supporting Information

ABSTRACT: The application of bimolecular reductive elimination to the activation of iron catalysts for alkene-diene cycloaddition is described. Key to this approach was the synthesis, characterization, electronic structure determination, and ultimately solution stability of a family of pyridine(diimine) iron methyl complexes with diverse steric properties and electronic ground states. Both the arylsubstituted, (MePDI)FeCH₃ and (EPDI)FeCH₃ (RPDI = 2,6-(2,6-R₂-C₆H₃N=CMe)₂C₅H₃N), and the alkyl-substituted examples, $(^{Cy}APDI)FeCH_3$ $(^{Cy}APDI = 2,6-(C_6H_{11}N=CMe)_2C_5H_3N)$, have

molecular structures significantly distorted from planarity and S = 3/2 ground states. The related N-arylated derivative bearing 2,6di-isopropyl aryl substituents, (iP PDI)FeCH₃, has an idealized planar geometry and exhibits spin crossover behavior from S = 1/2 to S = 3/2 states. At 23 °C under an N₂ atmosphere, both (MePDI)FeCH₃ and (EtPDI)FeCH₃ underwent reductive elimination of ethane to form the iron dinitrogen precatalysts, $[(^{Me}PDI)Fe(N_2)]_2(\mu-N_2)$ and $[(^{Et}PDI)Fe(N_2)]_2(\mu-N_2)$, respectively, while (iPrPDI)FeCH₃ proved inert to C-C bond formation. By contrast, addition of butadiene to all three iron methyl complexes induced ethane formation and generated the corresponding iron butadiene complexes, $(^{R}PDI)Fe(\eta^{4}-C_{4}H_{6})$ (R = Me, Et, ^{i}Pr), known precatalysts for the [2+2] cycloaddition of olefins and dienes. Kinetic, crossover experiments, and structural studies were combined with magnetic measurements and Mössbauer spectroscopy to elucidate the electronic and steric features of the iron complexes that enable this unusual reductive elimination and precatalyst activation pathway. Transmetalation of methyl groups between iron centers was fast at ambient temperature and independent of steric environment or spin state, while the intermediate dimer underwent the sterically controlled rate-determining reaction with either N_2 or butadiene to access a catalytically active iron compound.

INTRODUCTION

The formation of carbon-carbon bonds promoted by pyridine(diimine) iron complexes has enabled the synthesis of a broad scope of molecular architectures ranging from polymers to small molecules containing cyclobutyl groups. Independent, pioneering studies by Brookhart and Gibson reported that activation of aryl-substituted pyridine(diimine) iron dihalide complexes with methylaluminoxane (MAO) generated active precatalysts for the polymerization of ethylene (Scheme 1A). 2-6 Since these discoveries, considerable effort has been devoted to establishing structure-activity relationships through ligand alteration^{7,8} as well as establishing the identity and electronic structure of the propagating species responsible for C-C bond formation.

Insights into catalytically relevant intermediates have been investigated with the goal of improving the activity and selectivity of polymerization; however, the presence of excess MAO and the potential paramagnetism of the iron catalysts have posed challenges. ^{10–12} While early experimental ¹³ and theoretical¹⁴ proposals suggested low-spin iron(II) alkyl cations as the propagating species, it is now well-established

that the S = 2 spin state of the iron(II) dihalide is preserved upon generation of the cationic pyridine(diimine)iron alkyl active species. 15-18

Odd-electron, neutral pyridine(diimine) iron alkyl complexes have also demonstrated C-C bond-forming activity. 19,20 For example, Talsi and co-workers obtained evidence for the formation of iron alkyl complexes as intermediates in the polymerization of ethylene. 2,12 Cámpora and co-workers reported the oligomerization of ethylene from the neutral pyridine(diimine) iron methyl complex (iPrPDI)FeCH3 and conducted ¹H NMR spectroscopic studies to observe intermediates consistent with an associative coordinationinsertion mechanism.²¹ In both cationic and neutral pyridine-

Received: October 4, 2022 Published: February 23, 2023 I A C S



Scheme 1. Selected Examples of [(PDI)Fe]-Catalyzed C-C Bond Formation.^{30,31}

A. In Situ Activation of (PDI)Fe: Ethylene Polymerization

◆ Readily modified and tunable ligand ◆ Generalized method of activation

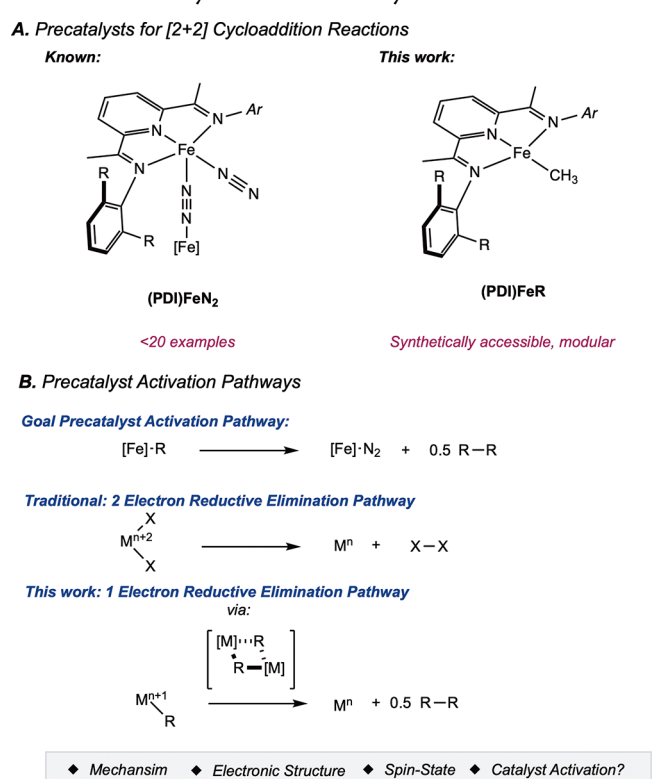
B. Well-Defined Formally Fe(0) [(PDI)Fe]: [2+2] Cycloaddition

(diimine) iron complexes, electronic and chemical participation of the ligand was either directly observed or implicated. $^{22-24}$

In addition to iron alkyl complexes, five-coordinate pyridine(diimine) formally iron(0) complexes have been synthesized and are active for a range of intra-²⁵ and intermolecular^{26–33} cycloaddition reactions of unactivated alkene–alkene, alkene–diene, and diene–diene partners (Scheme 1B). These include formation of unique C–C bond architectures containing cyclobutyl rings that are inaccessible by thermal, uncatalyzed pathways. Unlike polymerization catalysis, the number of suitable pyridine(diimine) compounds synthetically accessible to initiate C–C bond formation by cycloaddition has been limited due to the inaccessibility of a broad range of formally iron(0) precursors.

Pyridine(diimine) ligands are relatively straightforward to prepare, are sterically and electronically modular, 34-37 and offer the potential to support a host of electronically and sterically distinct structures. Despite the availability of ligand variants, catalytically active iron complexes, more specifically iron dinitrogen complexes, for unique cycloaddition reactions remain limited (Scheme 2). By contrast, pyridine(diimine) iron alkyl complexes are readily synthesized from the corresponding dihalide precursors. Conversion of these formally iron(I) derivatives to catalytically active iron(0) compounds would be transformative in expanding the scope of the latter and in establishing structure-reactivity relationships, especially with respect to the role of the redox-active chelate.² Inspiration for these studies derived from the observation that addition of excess propylene to meso-(tBuPDI)FeCH3, the corresponding dinitrogen complex of which is synthetically inaccessible, resulted in tail-to-tail dimerization, consistent with formation of a metallocyclopentane that undergoes β -hydride elimination and C-H reductive elimination.²⁹ In contrast to more traditional and well-studied two-electron reductive elimination, the desired transformation is a one-electron process and likely relies on the redox-active pyridine(diimine) ligand. Thus, mechanistic insight requires a detailed understanding of the electronic and molecular structures of pyridine(diimine) iron methyl complexes, which is presently lacking.

Scheme 2. One-Electron Reductive Elimination as a Method to Access Iron Cycloaddition Catalysts



Here we describe the application of bimolecular reductive elimination from pyridine(diimine) iron methyl complexes to generate a catalytically active iron complex for [2+2] cycloaddition. The electronic and molecular structures of the iron methyl precursors were comprehensively studied, and in one case, ($^{\rm iPr}PDI$)FeCH $_3$, spin-crossover behavior was observed. For each organometallic complex examined, transmetalation of methyl groups was fast at room temperature and independent of spin state and steric environment. Kinetic studies established an associative reaction with an incoming ligand, either N $_2$ or butadiene, that is rate determining for ethane formation.

■ RESULTS AND DISCUSSION

Synthesis and Solution Stability of Pyridine(diimine) Iron Methyl Complexes. The synthesis of (RPDI)FeCH₃ (R = iPr, Et) derivatives was reported from addition of methyllithium to the corresponding pyridine(diimine) iron dihalides.³⁸ Applying these procedures to the synthesis of (MePDI)FeCH₃ resulted in a mixture of the targeted methyl derivative along with the dinitrogen complex, [(MePDI)Fe- $(N_2)_2(\mu-N_2)$. Modifying the methylation procedure to dropwise addition of methyllithium to a solution of (MePDI)-FeCl₂ and to a shorter reaction time of 10 min resulted in the isolation of pure (MePDI)FeCH3 in 86% yield (Scheme 3A) as judged by ¹H NMR and ⁵⁷Fe Mössbauer spectroscopies. This synthetic route also minimized formation of byproducts, including bis(chelate) iron derivatives.³⁹ An analogous procedure was used to synthesize an example with an Nalkyl imine substituent, $({}^{Cy}APDI)FeCH_3$ (Scheme 3B). The observation of $[({}^{Me}PDI)Fe(N_2)]_2(\mu-N_2)$ at prolonged

The observation of $[(^{Me}PDI)Fe(N_2)]_2(\mu-N_2)$ at prolonged reaction times during the synthesis of $(^{Me}PDI)FeCH_3$ motivated a more comprehensive study into the solution

Scheme 3. Synthesis of (RPDI)FeCH₃ (R = Me, Et, Pr) and (CyAPDI)FeCH3 Complexes

A. Synthesis of (RPDI)FeCH3 Complexes

B. Synthesis of (CyAPDI)FeCH3

stability and geometric and electronic structures of pyridine-(diimine) iron alkyl complexes. Monitoring 0.8 mM benzene d_6 solutions of (${}^{R}PDI$)FeCH₃ (R = Et, Me) by ${}^{1}H$ NMR spectroscopy with cobaltocene as an internal paramagnetic standard sealed in a capillary at 23 °C revealed smooth conversion of the iron alkyl complex to $[(^{R}PDI)Fe(N_{2})]_{2}(\mu$ -N₂) with concomitant appearance of a resonance at 0.8 ppm corresponding to ethane. From these experiments, half-lives of 5 h and 5 days were measured for (MePDI)FeCH3 and (EtPDI)FeCH₃, respectively (Scheme 4). By contrast, (iPrPDI)-FeCH₃ was previously reported to be stable for weeks in benzene- d_6 solution at 23 °C and was confirmed in the present study. 40 The half-life of (CyAPDI)FeCH3 was also measured and was found to be approximately 3 days at room temperature. Unlike the N-arylated examples that provide ethane and a single, well-defined iron product, the consumption of (CyAPDI)FeCH3 was accompanied by formation of ethane, methane, the bis(chelate) iron complex (^{Cy}APDI)₂Fe, and free iron.

The unusual reductive elimination of ethane from the arylated pyridine(diimine) iron methyl compounds prompted additional studies to gain insight into the mechanism of the reaction. The net transformation is unusual in that it results in a net one-electron reduction of the iron, whereas more traditional reductive elimination processes are two-electron reduction processes. Nevertheless, this transformation is potentially valuable as a means to convert readily prepared iron alkyl compounds to catalytically active iron precursors.

Solid-State Structures of Pyridine(diimine) Iron **Methyl Complexes.** The solid-state structure of (iPrPDI)-FeCH₃ was reported previously and established an idealized planar molecule.³² The molecular structure of (CyAPDI)FeCH₃ was determined by X-ray diffraction, and a more distorted geometry was observed where the N(2)-Fe-C(22) angle is contracted to 147.0(1)° (Figure 1, left). A similar geometry was observed with (EtPDI)FeCH₃, where an N(2)-Fe1-C(30) angle of 156.2(2)° was observed in the structure recorded at 100 K (Figure 1, middle). By contrast, the N(2)-Fe(1)-C(34) angle for (iPrPDI)FeCH₃ is 179.3(1)° at 100 K, establishing the role of the large aryl substituents in enforcing planarity (Figure 1, right). Attempts to obtain a single crystal

Scheme 4. Relative Solution Stabilities of (RPDI)FeCH₃ and (CyAPDI)FeCH₃ Complexes under an N₂ Atmosphere

$$t_{1/2} = 5 \text{ hours}$$

$$t_{1/2} = 3 \text{ days}$$

$$t_{1/2} = 5 \text{ days}$$

of (MePDI)FeCH3 by recrystallization from pentane yielded $[(^{Me}PDI)Fe(N_2)]_2(\mu-N_2)$, likely due to facile reductive elimination of ethane in solution. However, the methyl group is assumed to also deviate from planarity due to the reduced steric environment around the metal alkyl. The lack of structural data for all four compounds in the series motivated additional spectroscopic, magnetic, and computational studies to further characterize the ground states of these compounds.

Spectroscopic, Magnetic, and Electronic Structure **Studies.** The benzene-d₆ ¹H NMR spectra of (MePDI)FeCH₃, (EtPDI)FeCH₃, (CyAPDI)FeCH₃, and (iPrPDI)FeCH₃ at 23 °C exhibit the number of resonances expected for $C_{2\nu}$ symmetric molecules. The chemical shift dispersions for (MePDI)FeCH₃ and (EtPDI)FeCH3 were observed over a 430 ppm range with the imine methyl groups appearing at -164.3 and -165.9 ppm, respectively, and the 4-pyridine hydrogens assigned at 265.6 and 263.1 ppm, respectively. The N-alkylated example, (CyAPDI)FeCH₃, exhibited similar features with resonances located over a 475 ppm range with the imine methyl group at -164.2 ppm and the proton in the 4-position of the pyridine appearing at 315.4 ppm. By contrast, (iPrPDI)FeCH₃ exhibits a slightly narrower chemical shift dispersion of 380 ppm with peaks observed between -163.8 and 216.5 ppm in benzene- d_6 at 23 °C. These differences in ¹H NMR shifts suggested possible differences in the electronic structures and molecular geometries among the series of iron methyl derivatives in solution.

The magnetic properties of each of the iron methyl complexes were examined with a combination of solution

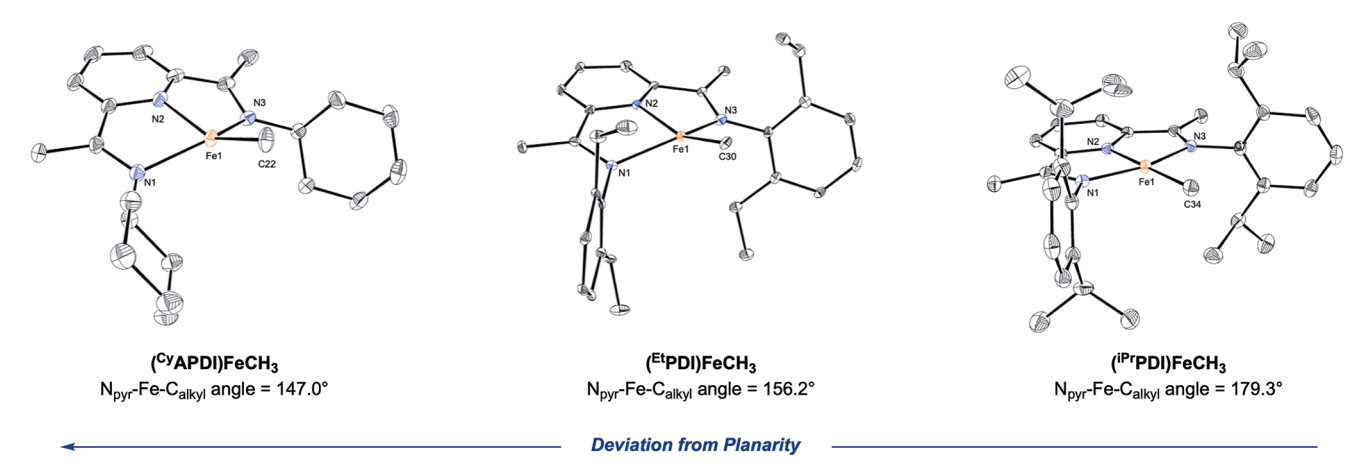


Figure 1. Solid-state structures from left to right of (CyAPDI)FeCH₃, (EtPDI)FeCH₃, and (iPrPDI)FeCH₃ at 30% probability ellipsoids. Hydrogen atoms are omitted for clarity.

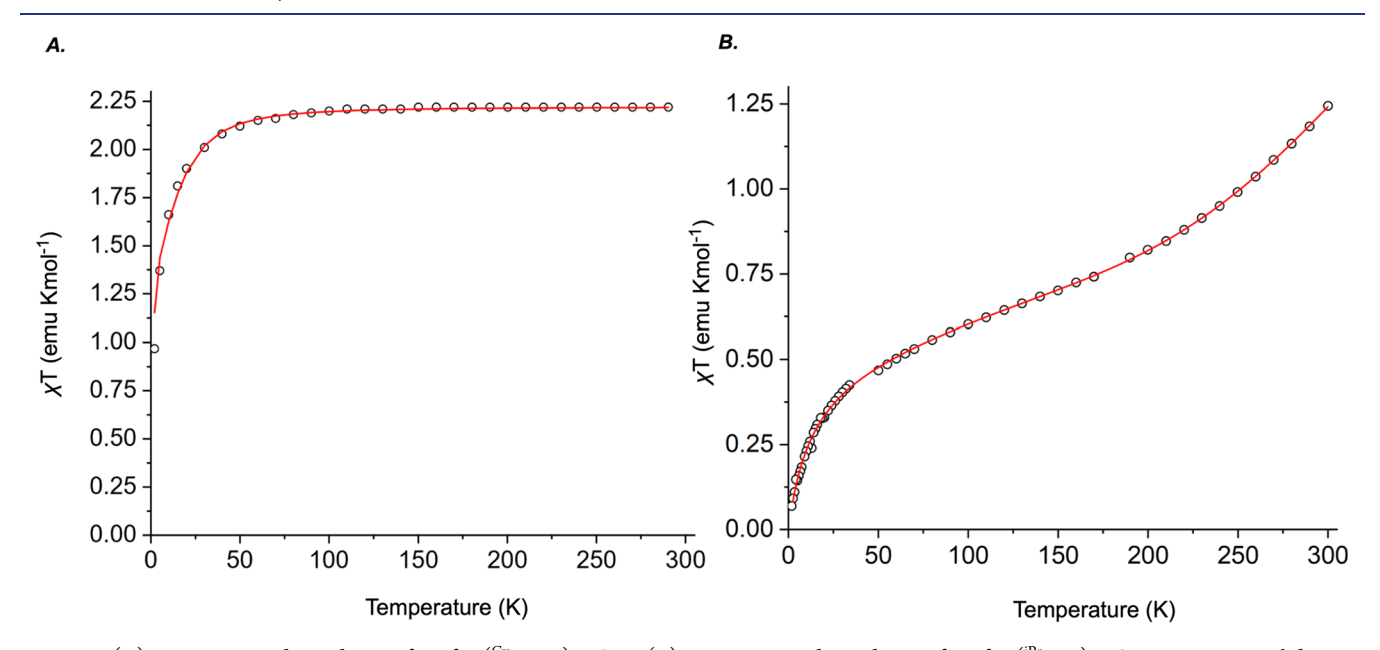


Figure 2. (A) Temperature dependence of χT for ($^{\text{Cy}}\text{APDI}$)FeCH $_3$. (B) Temperature dependence of χT for ($^{\text{IP}}\text{PDI}$)FeCH $_3$. Experimental data are represented by open circles; the red line shows the best theoretical fit. The fitting procedure and best-fit parameters are provided in the SI.

and solid-state measurements. Solution and solid state magnetic moments of 3.8 μ B and 3.9 μ B were measured for (MePDI)FeCH₃ and (CyAPDI)FeCH₃, respectively, at 23 °C. These values are consistent with the benzene- d_6 magnetic moment of 4.1 μ B for (EtPDI)FeCH₃ at 23 °C. These values are consistent with the spin-only value expected for three unpaired electrons and support high-spin iron centers. By contrast, a lower value of 3.5 μ B was measured for (iPrPDI)FeCH₃ under identical solution-state conditions. The anomalous magnetic moment coupled with the distinct molecular geometry and ¹H NMR shifts prompted a more thorough investigation of the magnetic properties of the compound. The spin-order response of the compound.

Measurements of magnetic susceptibility (χ) vs temperature (T) were conducted on solid samples of ($^{\text{Cy}}$ APDI)FeCH₃ and ($^{^{\text{IP}}}$ PDI)FeCH₃ using SQUID magnetometry. The SQUID data for ($^{\text{Cy}}$ APDI)FeCH₃, presented in Figure 2A, were collected as a reference for a high-spin iron derivative. As anticipated, simple paramagnetic behavior was observed with a plateau in moment at 4.2 μ_{B} ($\chi T = 2.21 \text{ emu·K·mol}^{-1}$). The data were successfully modeled using a spin-Hamiltonian for S

= 3/2, with the Lande factor g = 2.18 and the axial zero-field splitting parameter D = -20.0 cm⁻¹.

The data for (^{iP}PDI)FeCH₃ were collected over a similar temperature range, and a plot of χT as a function of temperature is presented in Figure 2B. The dependence is most consistent with spin-crossover behavior between S=1/2 and S=3/2 states, which result from antiferromagnetic (AFM) coupling between the spins on the Fe(II) center and the ligand-based radical (*vide infra*). In addition, a contribution of temperature-independent paramagnetism (χ_{TIP}) is also evident in the middle of the temperature range studied, and AFM intermolecular interactions (zJ) influence the χT values below 50 K.

The magnetic behavior of (iPrPDI)FeCH₃ was modeled using a common thermodynamic approach to a system that undergoes temperature-induced crossover between two states (see Supporting Information for details).⁴² The calculated value of magnetic susceptibility (χ_{calc}) is expressed as a combination of χ values for S=3/2 and S=1/2 states, with the contribution from the higher-entropy S=3/2 state becoming more pronounced with increasing temperature. The

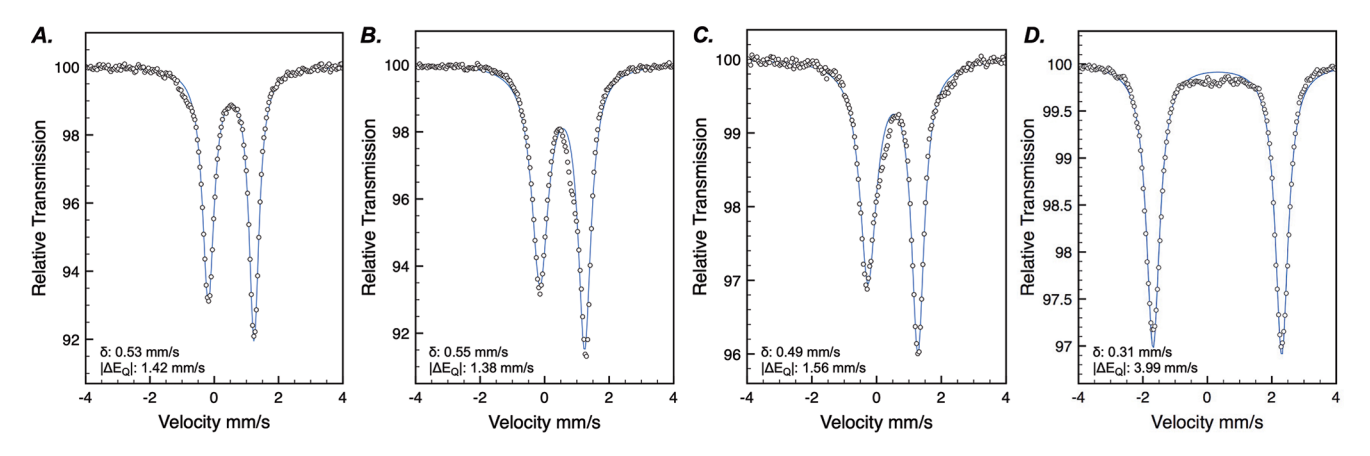


Figure 3. Solid-state, zero-field ⁵⁷Fe Mössbauer spectra of (A) (MePDI)FeCH₃, (B) (CyAPDI)FeCH₃, (C) (EtPDI)FeCH₃, and (D) (PPDI)FeCH₃ at 80 K. Open circles represent experimentally obtained data. Blue lines correspond to the fit of the data to the quadrupole doublets.

best fit to the experimental data gave the average spin crossover temperature, $T_{1/2} = 458(23)$ K, $\chi_{\rm TIP} = 1.68(1) \times 10^{-2}$ emu·mol⁻¹, and zJ = -19(1) cm⁻¹. The low accuracy of the $T_{1/2}$ value is explained by the lack of sufficient data in the higher-temperature region. Also noteworthy is the rather large negative value of zJ, suggesting substantial AFM interactions between the molecules in the solid state. This effect likely stems from the redox activity of the ligand, which leads to delocalization of the spin density closer to the periphery of the molecule, but it is also possible that the value of zJ incorporates spin—orbit coupling effects for the S = 1/2 state.

Zero-field ⁵⁷Fe Mössbauer spectroscopic data were collected on all four pyridine(diimine) iron methyl compounds. Spectra of (MePDI)FeCH₃, (CyAPDI)FeCH₃, (EtPDI)FeCH₃, and (iPPDI)FeCH₃, recorded at 80 K, are presented in Figure 3. The experimentally determined spectroscopic parameters along with related reference compounds are presented in Table 1. Isomer shifts of 0.53, 0.55, and 0.49 mm/s were

Table 1. Selected Experimental Zero-Field ⁵⁷Fe Mössbauer Parameters for (RPDI)FeCH₃ Complexes and Assignment of Spectroscopic Oxidation States

[Fe]	$\delta (\text{mm/s})$	$ \Delta E_{\rm Q} \ ({\rm mm/s})$	Ox. State
(MePDI)FeCH3 ^a	0.53	1.42	Fe(II), $S_{\text{Total}} = 3/2$
(CyAPDI)FeCH ₃	0.55	1.38	$Fe(II) S_{Total} = 3/2$
(EtPDI)FeCH ₃ ^a	0.49	1.56	Fe(II), $S_{\text{Total}} = 3/2$
(iPrPDI)FeCH ₃ ^a	0.31	3.99	SCO
(EtPDI)FeCH ₂ CMe ₃ ^b	0.56	1.13	Fe(II), $S_{\text{Total}} = 3/2$
(^{iPr} PDI)FeCH ₂ CMe ₃ ^b	0.57	1.16	Fe(II), $S_{\text{Total}} = 3/2$
(^{iPr} PDI)FeCH ₂ SiMe ₃ ^b	0.54	1.54	Fe(II), $S_{\text{Total}} = 3/2$

^aMeasurements on solid-state samples were performed at 80 K. ^bData were obtained from ref 15.

measured for (MepDI)FeCH₃, (CyAPDI)FeCH₃, and (EtpDI)FeCH₃, respectively, and are similar to those previously reported for (EtpDI)FeCH₂CMe₃, (iPrpDI)FeCH₂CMe₃, and (iPrpDI)FeCH₂SiMe₃. In contrast to (iPrpDI)FeCH₃, the solid-state structure of (EtpDI)FeCH₂CMe₃ is distorted where the alkyl ligand is lifted by 142.24(14)° from the idealized iron—chelate plane. These comparisons suggest that (MepDI)FeCH₃ also exhibits distortions from the planar geometry. By contrast, the zero-field, Fe Mössbauer spectrum of (iPrpDI)FeCH₃ exhibits a lower isomer shift of 0.31 mm/s at 80 K, further corroborating a difference in electronic structure

between the iron methyl variants. Likewise, this compound exhibits a larger quadrupole splitting of 3.99 mm/s, consistent with a planar geometry at iron. Because crystals suitable for X-ray diffraction were not obtained for (MepDI)FeCH₃, Mössbauer parameters were calculated for both square-planar and lifted geometries. The parameters obtained for the distorted geometries were comparable to the experimentally determined value, within error limits, while the planar geometry of (MepDI)FeCH₃ resulted in an uncharacteristically high quadrupole splitting of 2.19 mm/s, further supporting the distorted geometry of the complexes with less hindered substituents in the 2,6-aryl groups.

Summary of X-ray Emission Spectroscopy. The structural and electronic variations associated with the temperature change were further examined with Fe KB X-ray emission spectroscopy (XES), which probes relaxation of a 3p electron to a 1s hole following excitation of the 1s electron. $K\beta$ XES has previously shown sensitivity toward spin state and ligand oxidation state, 44-46 including in PDI iron complexes, but has not been widely applied for SCO systems. 48-50 In particular, the main line (~7060 eV for Fe) is highly sensitive toward spin state⁵¹ and shifted by 0.4 eV to higher energy in (iPrPDI)Fe(biphenyl)52 with a concomitant change in magnetic moment from 0.4 to 0.6 $\mu_{\rm B}$. Because XES is a molecular technique, a change in the energy of the $K\beta'$ detects a change in local Fe spin state, while being insensitive to long-range magnetic effects as is the case for SQUID. The reversible variable-temperature Kβ XES of (iPrPDI)FeCH₃ was collected at 100 and 298 K (Figure 4), and complete spectroscopic details and fits are reported in the Supporting Information. The $K\beta_{1,3}$ maximum is shifted 0.8 eV higher in energy for the roomtemperature sample (7060.06(2) eV) than for the sample at 100 K (7059.23(0) eV), supporting a higher spin state at room temperature. These observations support that the spin state change is a molecular event and are in agreement with the SQUID and Mössbauer spectroscopic studies. The data support an S = 1/2 state for (^{iPr}PDI)FeCH₃ below 100 K and a higher (S = 3/2) spin state that is populated at higher temperatures. Additionally, this study demonstrates the efficacy of using $K\beta$ XES for probing spin-state changes in spincrossover compounds.

Computational Studies. Density functional theory (DFT) calculations were performed using the B3LYP functional to gain insight into the electronic structure of this series of pyridine(diimine) iron methyl compounds. Only the most

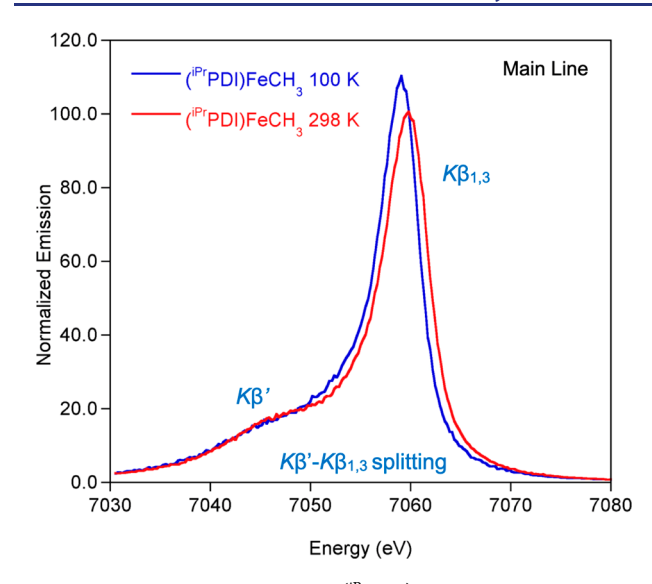


Figure 4. Fe K β XES mainlines of (iPrPDI)FeCH₃ at 100 and 298 K.

salient outputs are described here; complete computational studies and details are reported in the Supporting Information. The electronic structure description accounting for the limits of the spin crossover behavior for (iPPDI)FeCH₃ is reported in Figure 5. All calculations were performed using the full molecule to account for the steric effects of the isopropyl aryl groups.

The S=1/2 form of the compound with the idealized planar geometry is best described as intermediate spin ferrous ($S_{\rm Fe}=1$) engaged in antiferromagnetic coupling with a pyridine-(diimine) radical anion. Lifting of the methyl group from the idealized metal-chelate plane is accompanied by a change in electronic structure. While the pyridine-(diimine) ligand maintains its radical anion form, the ferrous ion changes from intermediate ($S_{\rm Fe}=1$) to high spin ($S_{\rm Fe}=2$), accounting for the overall S=3/2 state. These electronic structure descriptions are as expected from the observed geometries (e.g., planar complexes are intermediate-spin ferrous while distorted are high spin) and spectroscopic parameters and are consistent with the results of magnetic measurements on the solid-state sample.

Mechanistic Studies. With detailed electronic structure descriptions of both planar and lifted pyridine(diimine) iron methyl compounds in hand, we proceeded to investigate the mechanism of the unusual reductive elimination with the goal of understanding a new mode of catalyst activation. Two limiting mechanisms were considered: (i) radical homolysis of the iron alkyl bond and (ii) bimolecular reductive elimination involving a bridged intermediate (Scheme 5).

The experimental rate law was determined by measuring the disappearance of the paramagnetic 1H NMR resonances of ($^{\text{Et}}\text{PDI}$)FeCH $_3$ as a function of time in benzene- d_6 at 23 °C in the presence of excess N $_2$. The ethyl-substituted variant was selected due to the convenience of the time course of the reaction, and concentrations were determined relative to a cobaltocene standard contained in a capillary. 53 The data were best fit using a second-order dependence on the starting iron methyl complex, and this behavior was reproduced with both 1 and 4 atm of dinitrogen (Figure 6). The observed steric effect is consistent with a bimolecular process whereby iron complexes with smaller 2,6-aryl substituents underwent more rapid ethane formation. The proposed bimetallic intermediate

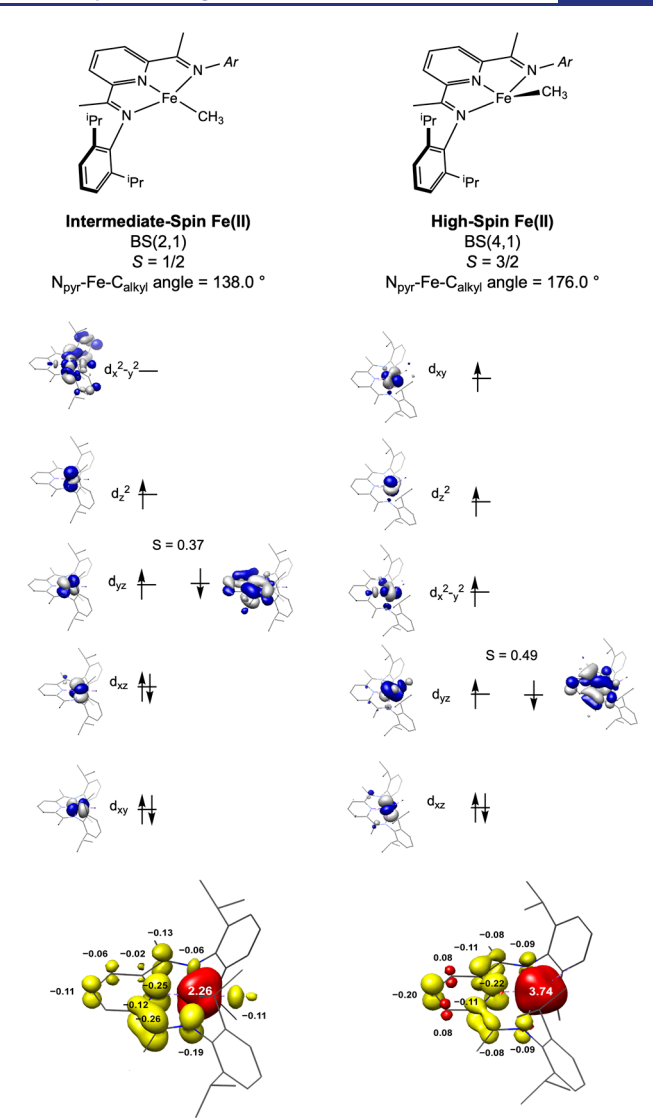


Figure 5. Top: Overview of computational solutions examined for the electronic structures of (^{iPr}PDI)FeCH₃. Middle: Qualitative molecular orbital diagram of (^{iPr}PDI)FeCH₃ (left) BS(2,1) calculation depicting localized orbitals using the B3LYP functional and (right) BS(4,1) calculation depicting localized orbitals using the B3LYP functional. Bottom: Spin density plot obtained from a Mulliken population analysis (left) for BS(2,1) (red: +2.26, yellow: −1.25) and (right) for BS(4,1) (red: +3.90, yellow: −0.98).

was not observed spectroscopically; however, an analogous intermediate was proposed for the isoelectronic cobalt methyl cation, 15-electron [(iPrPDI)CoCH₃][BArF₄], which also underwent bimolecular reductive elimination of ethane. In addition, Peters and co-workers proposed bimolecular reductive elimination of dihydrogen from iron thiolate compounds, forming bridging iron dinitrogen complexes.

The influence of N_2 on the rate of the reaction was also determined by monitoring the reaction time course by 1H NMR spectroscopy. Reaction vessels containing 1 and 4 atm of dinitrogen were monitored over the course of 15 days. A positive, non-zero-order dependence on N_2 (Figure 6A) was observed, consistent with interception of the bimetallic intermediate with dinitrogen in the rate-determining step. Solubility constants were used to determine the concentrations of N_2 in benzene assuming an ideal solution that obeys Henry's

Scheme 5. Mechanistic Possibilities Considered for Ethane Reductive Elimination from (RPDI)FeCH₃ Complexes

law. See Based on these approximations, the initial rate data established a first-order dependence on N_2 (Figure 6C).

To further assess the role of N_2 in the rate-determining step of the bimolecular reductive elimination, the stability of (EtPDI)FeCH3 in the absence of dinitrogen was investigated. Monitoring a benzene-d₆ solution of (EtPDI)FeCH₃ at 23 °C under vacuum revealed formation of ethane. However, the rate of disappearance of (EtPDI)FeCH3 was significantly diminished under vacuum, as indicated by its persistence in solution for an excess of 6 weeks. These data implicate dinitrogen as a coordinating ligand in the bimolecular reductive elimination of ethane. Additionally, hydrogen isotope exchange (HIE) was observed in the 4- and 3,5-positions of the pyridine, as well as the aryl group substituents (see Supporting Information). Activation of the benzene- d_6 solvent and reductive elimination of ethane in the absence of other L-type ligands is proposed to result in HIE. The observed H/D exchange has been previously reported for iron complexes bearing PDI ligands. ^{26,27,45,57}

To provide additional evidence for bimolecular reductive elimination and to further elucidate the mechanism, crossover experiments were conducted. These studies were also designed to inform on the relative rate of formation of the putative bimetallic intermediate and if this forms reversibly and faster than ethane. The deuterated isotopologues, (RPDI)FeCD₃ (R = Me, Et), were independently prepared by adapting the standard synthetic procedure with methyllilithium-d₃. Monitoring a benzene- d_6 solution containing an equimolar mixture of (MePDI)FeCH₃ and (EtPDI)FeCD₃ by ¹H NMR spectroscopy revealed the presence of two additional iron methyl compounds within 5 min as evidenced by the observation of four resolved 4-pyridine resonances (Scheme 6A). These resonances are consistent with the following isotopologues: (MePDI)FeCH₃, (MePDI)FeCD₃, (EtPDI)FeCH₃, and (EtPDI)-FeCD₃ (Scheme 6B). The formation and identification of (MePDI)FeCD3 was confirmed by independent synthesis. Continued reaction monitoring over the course of 24 h established generation of ethane- d_0 and ethane- d_3 , indicating that rapid iron methyl group exchange occurs significantly

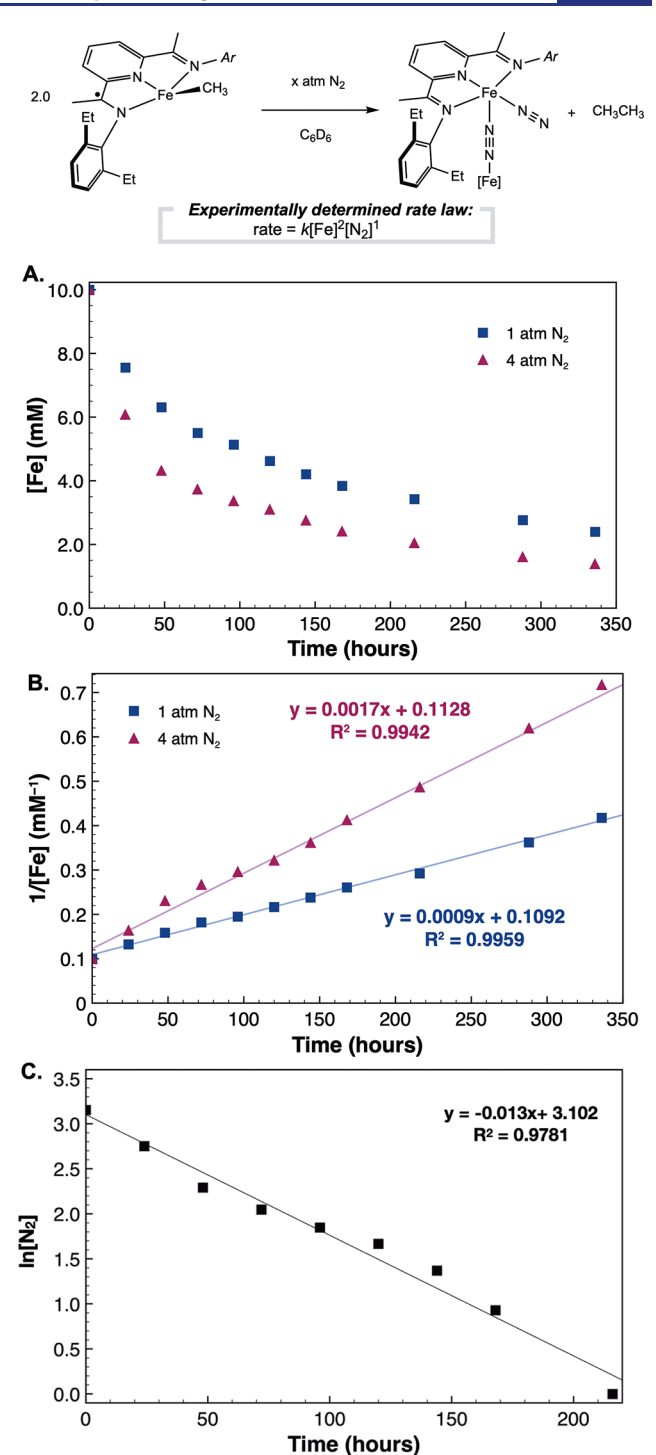
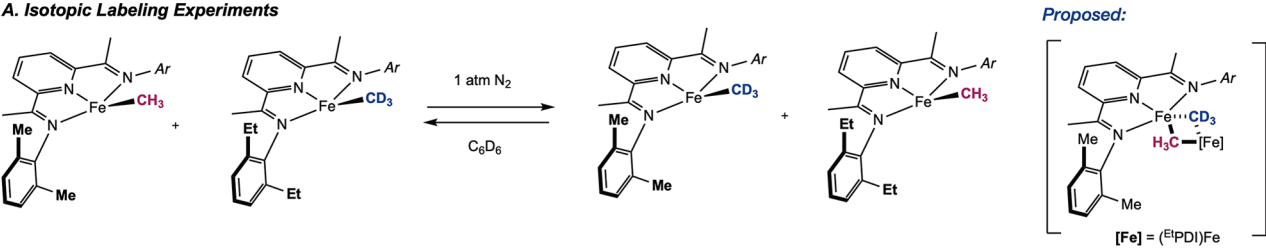


Figure 6. Top: Experimentally determined rate law for the bimolecular reductive elimination of ethane. (A) Plot of $[(^{Et}PDI)FeCH_3]$ vs time at varied concentrations of dinitrogen at ambient temperature. (B) Plot of $[(^{Et}PDI)FeCH_3]^{-1}$ vs time at 1 and 4 atm of dinitrogen. (C) Plot of $ln[N_2]$ vs time at 4 atm of dinitrogen.

faster than the rate of the bimolecular reductive elimination of ethane (Scheme 6C). Thus, formation of the bimetallic intermediate is fast and reversible and accounts for the exchange of the methyl groups. The reaction was repeated under vacuum, and methyl group exchange was still observed within 5 min, establishing that dinitrogen is not necessary for the formation of the proposed bimetallic intermediate. Analysis of the volatiles of the reductive elimination reaction conducted

Scheme 6. Methyl Group Exchange Monitored by Isotopic Labeling Studies

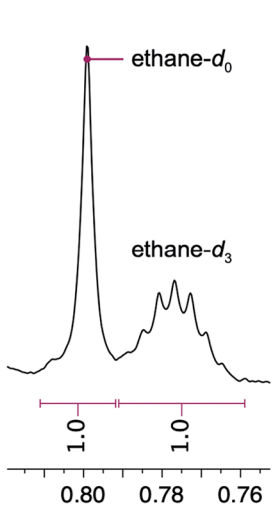
A. Isotopic Labeling Experiments



B. 4-Pyridine Resonances Corresponding to Each Isotopologue

4-pyridine resonances upon mixture of 1:1 (EtPDI)FeCD3 and (MePDI)FeCH3 in benzene-de authentic spectrum of (EtPDI)FeCD3 260.96 ppm authentic spectrum of (EtPDI)FeCH₃ 263.12 ppm authentic spectrum of (MePDI)FeCD3 264.44 ppm Magnithediaellepideographecisochipal authentic spectrum of (MePDI)FeCH3 265.55 ppm 265 260 255 f1 (ppm)

C. Volatiles Observed

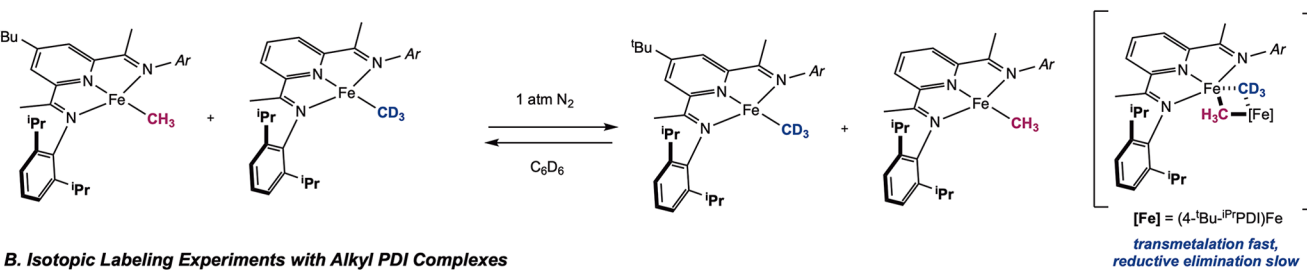


Ratio of Volatiles: 1:2:1 CH₃CH₃: CH₃CD₃: CD₃CD₃

Proposed:

Scheme 7. Transmetalation Monitored by Isotopic Labeling Studies

A. Isotopic Labeling Experiments with Sterically Hindered Aryl Substituents



under dinitrogen by ¹H NMR spectroscopy was consistent with a statistical mixture of ethane- d_0 , ethane- d_3 , and ethane- d_6 (Scheme 6C).

To better understand why (iPrPDI)FeCH3 was stable in solution, while the less hindered variants were not, the deuterated isotopologue (iPrPDI)FeCD3 was mixed with (4-tBu-iPrPDI)FeCH3. Characterization of (4-tBu-iPrPDI)-FeCH₃ revealed a planar geometry and electronic structure comparable to those of (iPrPDI)FeCH3. Upon dissolving a 2:1 mixture of (4-tBu-iPrPDI)FeCH3 to (iPrPDI)FeCD3 in benzened₆, ¹H NMR spectroscopy revealed the presence of four isotopologues (Scheme 7A). Because the distinct, isotopically sensitive NMR resonances correspond to the 4-pyridine position, two isotopologues of (^{iPr}PDI)FeCH₃ were observed. Evidence for the two isotopologues of (4-^tBu-^{iPr}PDI)FeCH₃ was obtained from the formation of two overlapping peaks corresponding to the protons of the imine backbone. The presence of these isotopologues was confirmed by the independent synthesis of (4-^tBu-^{iPr}PDI)FeCH₃. This finding established that the increased steric environment of the aryl substituents of (^{iPr}PDI)FeCH₃ did not prohibit or even detectably slow dimerization but it did influence the overall rate of reductive elimination. These findings established that transmetalation of aryl PDI iron methyl complexes is independent of ligand sterics.

To probe if the N-alkylated pyridine(diimine) iron methyl complex undergoes transmetalation, methyl group exchange was examined through a crossover experiment between ($^{\text{Cy}}\text{APDI}$)FeCH $_3$ and ($^{\text{iPr}}\text{PDI}$)FeCD $_3$ (Scheme 7B). An equimolar solution of ($^{\text{Cy}}\text{APDI}$)FeCH $_3$ and ($^{\text{iPr}}\text{PDI}$)FeCD $_3$ in benzene- d_6 was monitored by ^1H NMR spectroscopy. Two isotopologues of ($^{\text{iPr}}\text{PDI}$)FeCH $_3$ were observed within minutes, establishing fast transmetalation. After 1 h, the formation of the bis(chelate) iron complex among other products was observed, indicating that decomposition of ($^{\text{Cy}}\text{APDI}$)FeCH $_3$ was faster than reductive elimination.

To determine if the iron product following ethane reductive elimination from arylated pyridine(diimine) iron methyl complexes could be trapped with more catalytically relevant molecules, reactions with butadiene were examined. Addition of excess butadiene to a benzene- d_6 solution of (MePDI)FeCH₃ produced an immediate color change from green to red upon warming to ambient temperature. Analysis by ¹H NMR spectroscopy revealed >98% conversion of the iron methyl complex to the corresponding iron butadiene compound (Scheme 8). By comparison, the reaction of (iPrDI)FeCH₃ with excess butadiene in benzene- d_6 was slower; >98% conversion to (iPrDI)Fe(η^4 -C₄H₆) occurred within six hours.

Scheme 8. Reactivity of (PDI)FeCH₃ Complexes with Butadiene

To compare the preferred pathways of reductive elimination of iron methyl complexes in the presence of dinitrogen versus butadiene, kinetic studies were conducted for the conversion of ($^{\rm iPr}{\rm PDI}){\rm FeCH_3}$ to ($^{\rm iPr}{\rm PDI}){\rm Fe}(\eta^4{\rm -C_4H_6})$ (Figure 7). A second-order dependence on ($^{\rm iPr}{\rm PDI}){\rm FeCH_3}$ was determined in the same manner as described for ($^{\rm Et}{\rm PDI}){\rm FeCH_3}$. The disappearance of butadiene was measured with respect to mesitylene as a diamagnetic internal standard, and the data were best fit to a first-order dependence in butadiene, indicating that the rate law was consistent with different L-type ligands. The increased rate of reductive elimination observed with butadiene versus N_2 is likely a result of the greater nucleophilicity of the former

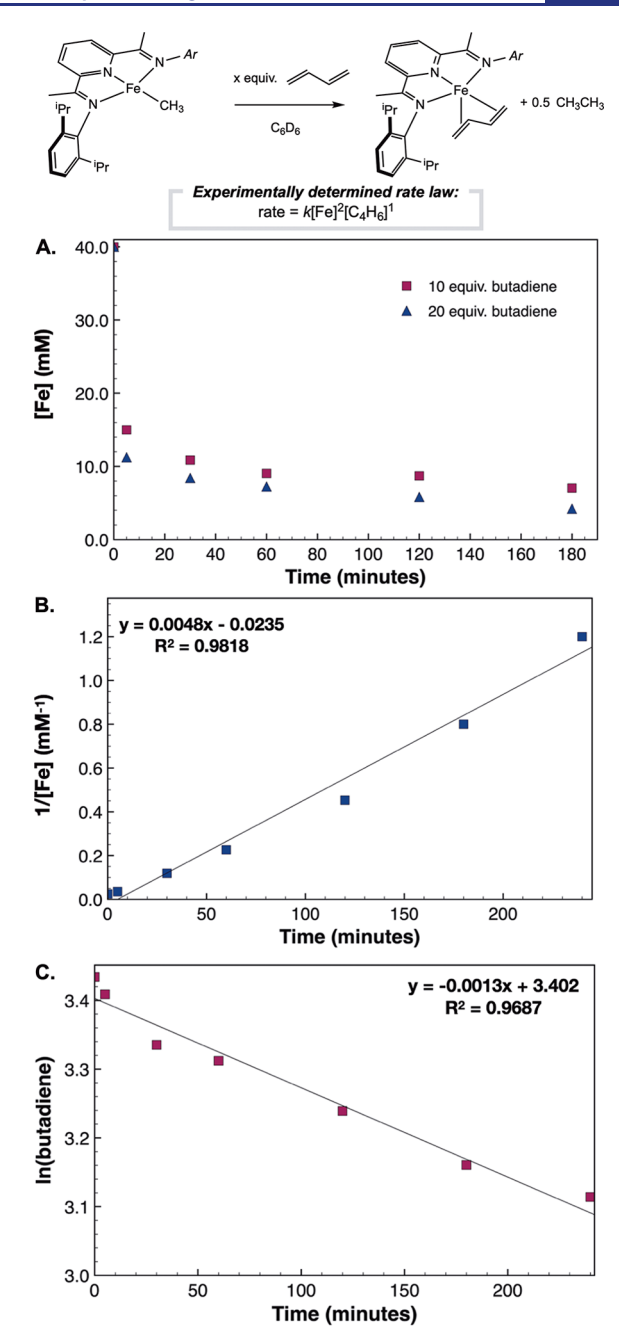


Figure 7. (A) Time course of conversion of ($^{\rm IP}$ rDI)FeCH $_3$ to ($^{\rm IP}$ rDI)Fe(η^4 -C $_4$ H $_6$). (B) Plot of $1/[(^{\rm IP}$ rDI)FeCH $_3]$ at 40 equiv of butadiene. (C) Plot of ln[butadiene] over time with 1 equiv of butadiene.

where butadiene is the more potent ligand and hence more effective in converting even low concentrations of the dimeric intermediate into formally iron(0) products.

Applications of Iron Methyl Complexes in [2+2] Cycloaddition Catalysis. With a generalized mechanism in hand, the pyridine(diimine) iron methyl complexes were applied to catalytic cycloaddition reactions. Catalytic conditions were adopted from previous reports of iron-catalyzed [2+2] cycloaddition reactions. Specifically, the [2+2] cycloaddition of ethylene and butadiene using (MepDI)FeCH₃ as the precatalyst was examined. Butadiene and ethylene were added sequentially to a benzene-d₆ solution containing 5 mol % (MepDI)FeCH₃ (Scheme 9A). Immediate formation of

Reductive Elimination Not Observed

Scheme 9. (A and B) [2+2]-Cycloaddition Reactions from Precatalyst (MePDI)FeCH₃; (C) Accessing Intermediates from (MePDI)FeCH₃ as a Precatalyst

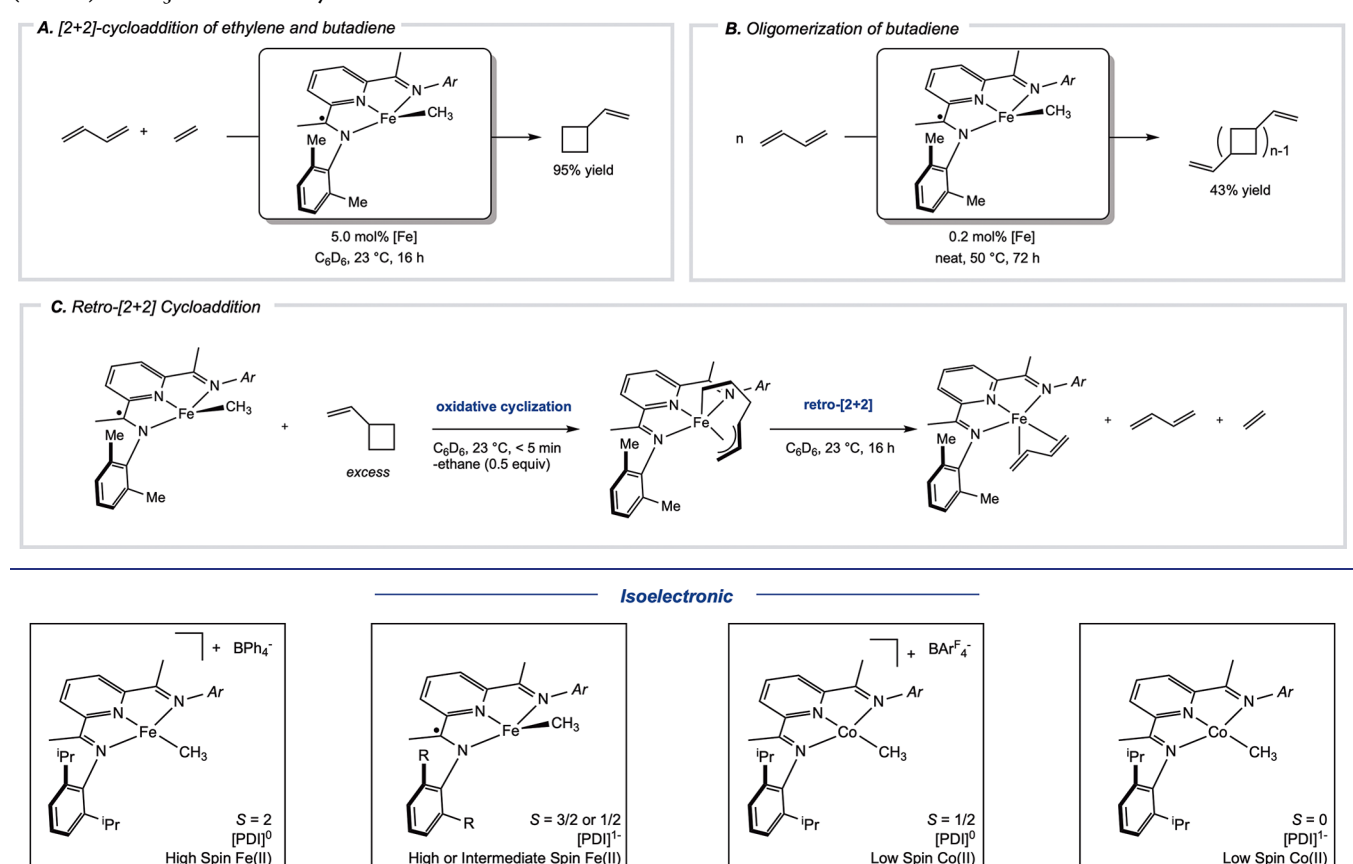
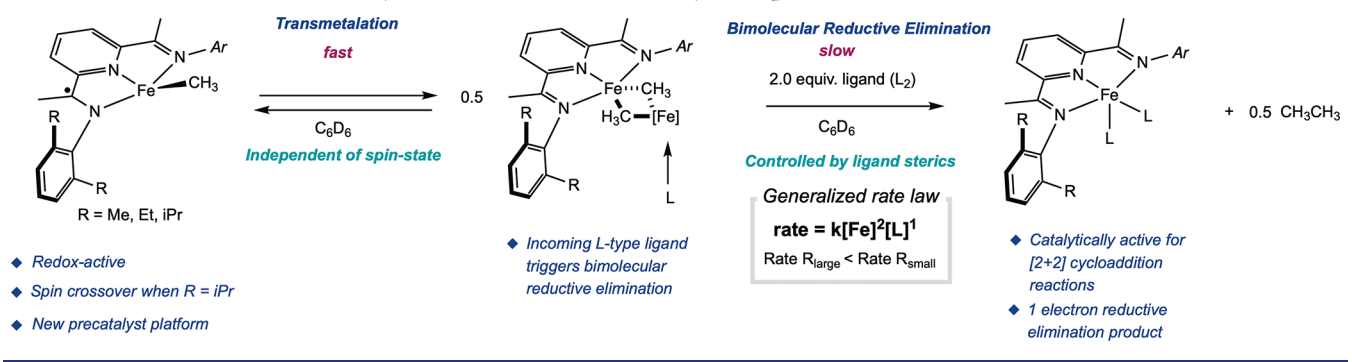


Figure 8. Neutral and cationic pyridine(diimine) metal-methyl complexes examined for reductive elimination of ethane.

Undergoes Bimolecular Reductive Elimination

Scheme 10. Neutral and Cationic Pyridine(diimine) Metal-Methyl Complexes Examined for Reductive Elimination of Ethane

Undergoes Bimolecular Reductive Elimination



 $(^{\text{Me}}\text{PDI})\text{Fe}(\eta^4\text{-}C_4\text{H}_6)$ was observed by ^1H NMR spectroscopy. The reaction was stirred for 16 h, at which time full conversion of ethylene and butadiene to vinylcyclobutane was observed, results that are consistent with those of the analogous pyridine(diimine) iron dinitrogen precatalyst. The homodimerization of butadiene was also examined from $(^{\text{Me}}\text{PDI})\text{FeCH}_3$, resulting in the synthesis of oligomers of (1,n'-divinyl)-oligocyclobutane in 43% yield (Scheme 9B).

With evidence of catalysis from the *in situ* activated (RPDI)FeCH₃ complex, the formation of reactive intermediates was explored through retro-[2+2] cycloaddition of vinylcyclobutane (Scheme 9C). The metallacyclic intermediate has been previously characterized, and ¹H NMR spectroscopy is useful for its detection during the course of the reaction. ²⁵

After 6 h, (MePDI)Fe(η^4 -C₄H₆) was observed as well as free butadiene and ethylene arising from retro-[2+2] cyclization. These results are consistent with those obtained in the reaction using [(MePDI)Fe(N₂)]₂(μ -N₂), indicating fast initiation from the iron methyl complexes. This work provides an alternative route to pyridine(diimine) iron precatalysts that are substrate activated, negating the need for activators or contaminants resulting from such activators. Notably, work by Thomas and co-workers provides a method for *in situ* activation of activated alkenes for [2+2] cycloaddition catalysis with sodium *tert*-butoxide, ⁵⁸ while this work provides access to the *in situ* activated [2+2] cycloaddition of unactivated substrates.

Requirements for Bimolecular Reductive Elimination of Ethane. The requirements of reductive elimination were

Reductive Elimination Not Observed

further explored to inform future precatalyst design and establish the generality of the transformation. Because pyridine(diimine) iron complexes have complex electronic structures involving ligand participation, understanding the influence of overall oxidation and spin state for the bimolecular reductive elimination of ethane was examined by observing the stability of the reported iron methyl complex [(iPrPDI)-FeCH₃][BPh₄].¹⁵ The solution stability of the complex was monitored for 24 h, and no reductive elimination was observed. In contrast, the previously reported, related cationic cobalt methyl complex, [(iPrPDI)CoCH₃][BArF₄], isoelectronic with the neutral iron methyl complexes, underwent reductive elimination of ethane upon addition of diethyl ether, which was proposed through a bimetallic pathway.⁵⁴ The planar, S = 1/2 cobalt cation provided additional evidence that non-zero spin state is not likely a necessary requirement for bimolecular reductive elimination. Fitting with the observed trend, the neutral, diamagnetic pyridine(diimine) cobalt methyl complex (iPrPDI)CoCH₃ did not undergo the reductive elimination of ethane, indicating that the electron count of the metal complex was relevant to determining reactivity (Figure 8).

Scheme 10 presents a summary of the mechanistic findings in this work. For all neutral pyridine(diimine) iron methyl complexes studied, transmetalation was fast at ambient temperature, independent of imine substituent, molecular geometry, or spin state. Reductive elimination of ethane is preferred with aryl-substituted ligands with relatively small substituents, as these facilitate formation of the bimetallic intermediate as well as productive cleavage with an incoming ligand. The more nucleophilic the ligand, the higher the rate of ethane formation. These steric and electronic structure requirements are preserved with isoelectronic, cationic cobalt methyl complexes upon addition of diethyl ether. Notably, oxidation or reduction from this preferred oxidation state inhibits the overall reaction.

CONCLUSIONS

A facile method for synthesizing iron alkyl complexes and subsequently accessing formally iron(0) complexes by bimolecular reductive elimination of ethane was developed. Detailed molecular and electronic structure studies were conducted on a series of iron methyl derivatives, and the role of the redox-active pyridine(diimine) ligand was elucidated. Geometries vary from idealized planar in the case with the largest 2,6-aryl substituents to highly distorted and high spin with the smallest substituents. Substituent effects on the iron complexes, the experimentally determined rate law, and isotopic labeling studies support a pathway involving formation of a diiron intermediate with bridging methyl groups ultimately resulting in loss of ethane. The overall electron count of the metal complex was the most important criterion for bimolecular reductive elimination rather than the spin-state or ground-state molecular geometry. This understanding of a fundamental organometallic transformation allowed access to iron butadiene or dinitrogen-containing precatalysts that are active for C-C bond-forming reactions and provides a framework for synthesizing other complexes capable of undergoing bimolecular reductive elimination to access catalytically active complexes.

ASSOCIATED CONTENT

Supporting Information

The Supporting Information is available free of charge at https://pubs.acs.org/doi/10.1021/jacs.2c10547.

Complete experimental details and characterization data including NMR spectra, magnetic data, X-ray emission data, and computational studies (PDF)

Accession Codes

CCDC 2181965–2181969 and 2226812–2226813 contain the supplementary crystallographic data for this paper. These data can be obtained free of charge via www.ccdc.cam.ac.uk/data_request/cif, or by emailing data_request@ccdc.cam.ac.uk, or by contacting The Cambridge Crystallographic Data Centre, 12 Union Road, Cambridge CB2 1EZ, UK; fax: +44 1223 336033.

AUTHOR INFORMATION

Corresponding Author

Paul J. Chirik — Department of Chemistry, Princeton University, Princeton, New Jersey 08544, United States; orcid.org/0000-0001-8473-2898; Email: pchirik@princeton.edu

Authors

Carli B. Kovel — Department of Chemistry, Princeton University, Princeton, New Jersey 08544, United States; orcid.org/0000-0001-6585-8129

Jonathan M. Darmon — Department of Chemistry, Princeton University, Princeton, New Jersey 08544, United States; orcid.org/0000-0002-2387-2958

S. Chantal E. Stieber – Department of Chemistry, Princeton University, Princeton, New Jersey 08544, United States;
ocid.org/0000-0003-3778-207X

Gisselle Pombar — Department of Chemistry, Princeton University, Princeton, New Jersey 08544, United States Tyler P. Pabst — Department of Chemistry, Princeton University, Princeton, New Jersey 08544, United States; orcid.org/0000-0003-4595-2833

Bastian Theis — Department of Chemistry, Princeton University, Princeton, New Jersey 08544, United States Zoë R. Turner — Department of Chemistry, Princeton University, Princeton, New Jersey 08544, United States; orcid.org/0000-0003-2044-9203

Ökten Üngör – Department of Chemistry and Biochemistry, Florida State University, Tallahassee, Florida 32306, United States; orcid.org/0000-0001-7071-6651

Michael Shatruk – Department of Chemistry and Biochemistry, Florida State University, Tallahassee, Florida 32306, United States; ocid.org/0000-0002-2883-4694

Serena DeBeer – Max Planck Institute for Chemical Energy Conversion, 45470 Mülheim an der Ruhr, Germany;
orcid.org/0000-0002-5196-3400

Complete contact information is available at: https://pubs.acs.org/10.1021/jacs.2c10547

Notes

The authors declare no competing financial interest.

ACKNOWLEDGMENTS

This research was supported by the U.S. Department of Energy, Office of Science, Office of Basic Energy Sciences, Catalysis Science program, under Award DE-SC0022303. S.D.

acknowledges the Max Planck Society for funding. S.C.E.S. thanks NSF GRFP and CAREER (1847926) for funding. Characterization of magnetic properties was performed with support from the National Science Foundation, Award CHE-1955754. The XES data were measured at the Center for High Energy X-ray Sciences (CHEXS), which is supported by the National Science Foundation under award DMR-1829070. We also thank Dr. Grant Marguileux for experimental assistance with X-ray diffraction, Megan Mohadjer Beromi for helpful discussion, and Dr. Istvan Pelczer and Kenneth Conover for guidance with NMR spectroscopy.

■ REFERENCES

- (1) Chirik, P. J. Carbon-Carbon Bond Formation in a Weak Ligand Field: Leveraging Open-Shell First-Row Transition Metal Catalysis. *Angew. Chem., Int. Ed.* **2017**, *56*, 5170–5181.
- (2) Soshnikov, I. E.; Semikolenova, N. V.; Bushmelev, A. N.; Bryliakov, K. P.; Lyakin, O. Y.; Redshaw, C.; Zakharov, V. A.; Talsi, E. P. Investigating the Nature of the Active Species in Bis(imino)-pyridine Cobalt Ethylene Polymerization Catalysts. *Organometallics* **2009**, *28*, 6003–6013.
- (3) Small, B. L.; Brookhart, M. Iron-Based Catalysts with Exceptionally High Activities and Selectivities for Oligomerization of Ethylene to Linear α -Olefins. *J. Am. Chem. Soc.* **1998**, *120*, 7143–7144.
- (4) Small, B. L.; Brookhart, M.; Bennett, A. M. A. Highly Active Iron and Cobalt Catalysts for the Polymerization of Ethylene. *J. Am. Chem. Soc.* **1998**, *120*, 4049–4050.
- (5) Britovsek, G. J.; Gibson, V. C.; McTavish, S. J.; Solan, G. A.; White, A. J.; Williams, D. J.; Kimberley, B. S.; Maddox, P. J. Novel Olefin Polymerization Catalysts Based on Iron and Cobalt. *Chem. Commun.* 1998, 849–850.
- (6) Britovsek, G. J. P.; Bruce, M.; Gibson, V. C.; Kimberley, B. S.; Maddox, P. J.; Mastroianni, S.; McTavish, S. J.; Redshaw, C.; Solan, G. A.; Strömberg, S.; White, A. J. P.; Williams, D. J. Iron and Cobalt Ethylene Polymerization Catalysts Bearing 2,6-Bis(Imino)Pyridyl Ligands: Synthesis, Structures, and Polymerization Studies. *J. Am. Chem. Soc.* 1999, 121, 8728–8740.
- (7) Gibson, V. C.; Redshaw, C.; Solan, G. A. Bis(imino)pyridines: Surprisingly Reactive Ligands and a Gateway to New Families of Catalysts. *Chem. Rev.* **2007**, *107*, 1745–1776.
- (8) Matsugi, T.; Fujita, T. High-Performance Olefin Polymerization Catalysts Discovered on the Basis of a New Catalyst Design Concept. *Chem. Soc. Rev.* **2008**, *37*, 1264–1277.
- (9) Small, B. L. Discovery and development of pyridine-bis(imine) and related catalysts for olefin polymerization and oligomerization. *Acc. Chem. Res.* **2015**, *48*, 2599–2611.
- (10) Scott, J.; Gambaraotta, S.; Korobkov, I.; Knijnenburg, Q.; de Bruin, B.; Budzelaar, P. H. M. Formation of a Paramagnetic Al Complex and Extrusion of Fe During the Reaction of (Diiminopyridine) Fe with AlR₃ (R = Me, Et). *J. Am. Chem. Soc.* **2005**, *127*, 17204–17206.
- (11) Cartes, M. A.; Rodriguez-Delgado, A.; Palma, P.; Alvarez, E.; Campora, J. Sequential Reduction and Alkyl Exchange Reactions of Bis(imino)pyridine Dialkyliron(II) with Triethylaluminum. *Organometallics* **2014**, *33*, 1834–1839.
- (12) Bryliakov, K. P.; Talsi, E. P.; Semikolenova, N. V.; Zakharov, V. A. Formation and Nature of the Active Sites in Bis(imino)pyridine Iron-Based Polymerization Catalysts. *Organometallics* **2009**, 28, 3225–3232.
- (13) Babik, S. T.; Fink, G. Propylene Polymerization with a Bisiminepyridine Iron Complex: Activation with $Ph_3C[B(C_6F_5)_4]$ and AlR_3 ; Iron Hydride Species in the Catalytic Cycle. *J. Mol. Catal. A* **2002**, *188*, 245–253.
- (14) Deng, L.; Margl, P.; Ziegler, T. Mechanistic Aspects of Ethylene Polymerization by Iron(II)-Bisimine Pyridine Catalysts: A Combined Density Functional Theory Molecular Mechanics Study. *J. Am. Chem. Soc.* 1999, 121, 6479–6487.

- (15) Tondreau, A. M.; Milsmann, C.; Patrick, A. D.; Hoyt, H. M.; Lobkovsky, E.; Wieghardt, K.; Chirik, P. J. Synthesis and Electronic Structure of Cationic, Neutral, and Anionic Bis(imino)pyridine Iron Alkyl Complexes: Evaluation of Redox Activity in Single-Component Ethylene Polymerization Catalysts. *J. Am. Chem. Soc.* **2010**, *132*, 15046–15059.
- (16) Bouwkamp, M. W.; Lobkovsky, E.; Chirik, P. J. Bis(imino)-pyridine Iron(II) Alkyl Cations for Olefin Polymerization. *J. Am. Chem. Soc.* **2005**, 127, 9660–9661.
- (17) Schaefer, B. A.; Margulieux; Tiedemann, M. A.; Small, B. L.; Chirik, P. J. Synthesis and electronic structure of iron borate betaine complexes as route to single-component iron ethylene oligomerization and polymerization catalysts. *Organometallics* **2015**, *34*, 5615–5623.
- (18) Chirik, P. J.; Schaefer, B. A.; Margulieux, G. W. Cationic Pyridine(diimine)iron Tethered Alkene Complexes: Synthetic Models for Elusive Intermediates in Iron-Catalyzed Ethylene Polymerization. *Bull. Japan Society of Coordination Chemistry* **2016**, *67*, 19–29.
- (19) Zhang, B.; Aguilera, M. C.; Cajiao, N.; Neidig, M. L. Recent Advances in Synthesis, Characterization and Reactivities of Iron-Alkyl and Iron-Aryl Complexes. In Reference Module in Chemistry, Molecular Sciences and Chemical Engineering; Elsevier, 2021.
- (20) Champouret, Y.; Hashmi, O. H.; Visseaux, M. Discrete ironbased complexes: Applications in Homogeneous Coordination Insertion Polymerization Catalysis. *Coord. Chem. Rev.* **2019**, 390, 127–170.
- (21) Ángeles Cartes, M.; Rodríguez-Delgado, A.; Palma, P.; Sánchez, L. J.; Cámpora, J. Direct Evidence for a Coordination—Insertion Mechanism of Ethylene Oligomerization Catalysed by Neutral 2,6-Bisiminopyridine Iron Monoalkyl Complexes. *Catal. Sci. Technol.* 2014, 4, 2504–2507.
- (22) Bart, S. C.; Chłopek, K.; Bill, E.; Bouwkamp, M. W.; Lobkovsky, E.; Neese, F.; Wieghardt, K.; Chirik, P. J. Electronic Structure of Bis(imino)pyridine Iron Dichloride, Monochloride, and Neutral Ligand Complexes: A Combined Structural, Spectroscopic, and Computational Study. *J. Am. Chem. Soc.* **2006**, *128*, 13901–13912.
- (23) Elsby, M. R.; Baker, R. T. Strategies and mechanisms of metalligand cooperativity in first-row transition metal complexes catalysts. *Chem. Soc. Rev.* **2020**, *49*, 8933–8987.
- (24) Romelt, C.; Weyhermuller, T.; Weighardt, K. Structural Characterisitcs of Redox-Active Pyridine-1,6-Diimine Complexes: Electronic Structures and Ligand Oxidation Levels. *Coord. Chem. Rev.* **2019**, 380, 287–317.
- (25) Bouwkamp, M. W.; Bowman, A. C.; Lobkovsky, E.; Chirik, P. J. Iron-Catalyzed $[2\pi + 2\pi]$ Cycloaddition of α,ω -Dienes: The Importance of Redox-Active Supporting Ligands. *J. Am. Chem. Soc.* **2006**, 128, 13340–13341.
- (26) Kennedy, C. R.; Joannou, M. V.; Steves, J. E.; Hoyt, J. M.; Kovel, C. B.; Chirik, P. J. Iron-Catalyzed Vinylsilane Dimerization and Cross-Cycloadditions with 1,3-Dienes: Probing the Origins of Chemo- and Regioselectivity. ACS Catal. 2021, 11, 1368–1379.
- (27) Joannou, M. V.; Hoyt, J. M.; Chirik, P. J. Investigations into the Mechanism of Inter- and Intramolecular Iron-Catalyzed [2 + 2] Cycloaddition of Alkenes. *J. Am. Chem. Soc.* **2020**, *142*, 5314–5330. (28) Beromi, M. M.; Younker, J. M.; Zhong, H.; Pabst, T. P.; Chirik, P. J. Catalyst Design Principles Enabling Intermolecular Alkene-Diene [2 + 2] Cycloaddition and Depolymerization Reactions. *J. Am. Chem. Soc.* **2021**, *143*, 17793–17805.
- (29) Hoyt, J. M.; Schmidt, V. A.; Tondreau, A. M.; Chirik, P. J. Iron-Catalyzed Intermolecular [2 + 2] Cycloadditions of Unactivated Alkenes. *Science* **2015**, *349*, 960–963.
- (30) Mohadjer Beromi, M.; Kennedy, C. R.; Younker, J. M.; Carpenter, A. E.; Mattler, S. J.; Throckmorton, J. A.; Chirik, P. J. Iron-Catalysed Synthesis and Chemical Recycling of Telechelic 1,3-Enchained Oligocyclobutanes. *Nat. Chem.* **2021**, *13*, 156–162.
- (31) Russell, S. K.; Lobkovsky, E.; Chirik, P. J. Iron-Catalyzed Intermolecular $[2\pi + 2\pi]$ Cycloaddition. *J. Am. Chem. Soc.* **2011**, *133*, 8858–8861.

- (32) Kennedy, C. R.; Zhong, H.; Macaulay, R. L.; Chirik, P. J. Regioand Diastereoselective Iron-Catalyzed [4 + 4]-Cycloaddition of 1,3-Dienes. *J. Am. Chem. Soc.* **2019**, *141*, 8557–8573.
- (33) Morris, D. M.; Quintana, R. L.; Harvey, B. G. High-Performance Jet Fuels Derived from Bio-Based Alkenes by Iron-Catalyzed [2+ 2] Cycloaddition. *ChemSusChem* **2019**, *12*, 1646–1652
- (34) Gygi, D.; Hwang, S. J.; Nocera, D. G. Scalable Syntheses of 4-Substituted Pyridine–Diimines. *J. Org. Chem.* **2017**, *82*, 12933–12938.
- (35) Römelt, C.; Weyhermüller, T.; Wieghardt, K. Structural Characteristics of Redox-Active Pyridine-1,6-Diimine Complexes: Electronic Structures and Ligand Oxidation Levels. *Coord. Chem. Rev.* **2019**, 380, 287–317.
- (36) Gibson, V. C.; Redshaw, C.; Solan, G. A. Bis(imino)pyridines: Surprisingly Reactive Ligands and a Gateway to New Families of Catalysts. *Chem. Rev.* **2007**, *107*, 1745–1776.
- (37) Doll, J. S.; Regenauer, N. I.; Bothe, V. P.; Wadepohl, H.; Roşca, D.-A. Redox Activity of Iron Diazine-Diimine Carbonyl and Dinitrogen Complexes: A Comparitive Study on the Influence of the Heterocyclic Ring. *Inorg. Chem.* **2022**, *61*, 520–532.
- (38) Bouwkamp, M. W.; Bart, S. C.; Hawrelak, E. J.; Trovitch, R. J.; Lobkovsky, E.; Chirik, P. J. Square Planar Bis(imino)pyridine Iron Halide and Alkyl Complexes. *Chem. Commun.* **2005**, *27*, 3406–3408.
- (39) Russell, S. K.; Darmon, J. M.; Lobkovsky, E.; Chirik, P. J. Synthesis of Aryl-Substituted Bis(imino)pyridine Iron Dinitrogen Complexes. *Inorg. Chem.* **2010**, 49, 2782–2792.
- (40) Trovitch, R. J.; Lobkovsky, E.; Chirik, P. J. Bis(Imino)Pyridine Iron Alkyls Containing Beta-Hydrogens: Synthesis, Evaluation of Kinetic Stability, and Decomposition Pathways Involving Chelate Participation. *J. Am. Chem. Soc.* **2008**, *130*, 11631–11640.
- (41) Evans, D. 400. The Determination of the Paramagnetic Susceptibility of Substances in Solution by Nuclear Magnetic Resonance. *J. Chem. Soc.* **1959**, 2003–2005.
- (42) König, E. Nature and Dynamics of the Spin-State Interconversion in Metal Complexes. *Struct. Bonding (Berlin)* **1991**, 76, 51–152.
- (43) Hawrelak, E. J.; Bernskoetter, W. H.; Lobkovsky, E.; Yee, G. T.; Bill, E.; Chirik, P. J. Square Planar vs Tetrahedral Geometry in Four Coordinate Iron(II) Complexes. *Inorg. Chem.* **2005**, *44*, 3103–3111.
- (44) Her, J. L.; Matsuda, Y. H.; Nakano, M.; Niwa, Y.; Inada, Y. J. Magnetic Field-Induced Spin-Crossover Transition in [Mn^{III}(taa)] Studied by X-Ray Absorption Spectroscopy. *Appl. Phys.* **2012**, *111*, No. 053921.
- (45) Glatzel, P.; Bergmann, U.; Glatzel, P.; Bergmann, U. High Resolution 1s Core Hole X-ray Spectroscopy in 3d Transition Metal Complexes—Electronic and Structural Information. *Coord. Chem. Rev.* 2005, 249, 65–95.
- (46) Phu, P. N.; Gutierrez, C. E.; Kundu, S.; Sokaras, D.; Kroll, T.; Warren, T. H.; Stieber, S. C. E. Quantification of Ni–N–O Bond Angles and NO Activation by X-ray Emission Spectroscopy. *Inorg. Chem.* **2021**, *60*, 736–744.
- (47) Stieber, S. C. E.; Milsmann, C.; Hoyt, J. M.; Turner, Z. R.; Finkelstein, K. D.; Wieghardt, K.; DeBeer, S.; Chirik, P. J. Bis(imino)pyridine Iron Dinitrogen Compounds Revisited: Differences in Electronic Structure Between Four- and Five-Coordinate Derivatives. *Inorg. Chem.* **2012**, *51*, 3770–3785.
- (48) Osawa, H.; Iwazumi, T.; Shoji, H.; Hirai, E.; Nakamura, T.; Ogawa, Y.; Ishikawa, T.; Koshihara, S.; Isozumi, Y.; Nanao, S. Spin-State Transitions in an Iron Spin-Crossover Complex Observed with X-ray Emission and X-ray Absorption. *Phase Transit.* **2002**, *75*, 919–925
- (49) Lin, J.-F.; Struzhkin, V. V.; Jacobsen, S. D.; Hu, M. Y.; Chow, P.; Kung, J.; Liu, H.; Mao, H.-k.; Hemley, R. J. Spin Transition of Iron in Magnesiowüstite in the Earth's Lower Mantle. *Nature* **2005**, *436*, 377–380.
- (50) Mebs, S.; Braun, B.; Kositzki, R.; Limberg, C.; Haumann, M. Abrupt Versus Gradual Spin-Crossover in FeII(phen)2(NCS)2 and FeIII(dedtc)3 Compared by X-Ray Absorption and Emission

- Spectroscopy and Quantum-Chemical Calculations. *Inorg. Chem.* **2015**, *54*, 11606–11624.
- (51) Lee, N.; Petrenko, T.; Bergmann, U.; Neese, F.; DeBeer, S. Probing Valence Orbital Composition with Iron $K\beta$ X-ray Emission Spectroscopy. *J. Am. Chem. Soc.* **2010**, 132, 9715–9727.
- (52) Darmon, J. M.; Stieber, S. C. E.; Sylvester, K. T.; Fernández, I.; Lobkovsky, E.; Semproni, S. P.; Bill, E.; Wieghardt, K.; DeBeer, S.; Chirik, P. J. Oxidative Addition of Carbon—Carbon Bonds with a Redox-Active Bis(imino)pyridine Iron Complex. *J. Am. Chem. Soc.* **2012**, *134*, 17125—17137.
- (53) Mohadjer Beromi, M.; Banerjee, G.; Brudvig, G. W.; Hazari, N.; Mercado, B. Q. Nickel(I) Aryl Species: Synthesis, Properties, and Catalytic Activity. ACS Catal. 2018, 8, 2526–2533.
- (54) Hojilla Atienza, C. C.; Milsmann, C.; Lobkovsky, E.; Chirik, P. J. Synthesis, Electronic Structure, and Ethylene Polymerization Activity of Bis(imino)pyridine Cobalt Alkyl Cations. *Angew. Chem., Int. Ed.* **2011**, *50*, 8143–8147.
- (55) Gu, N. X.; Oyala, P. H.; Peters, J. C. An S = 1/2 Iron Complex Featuring N_2 , Thiolate, and Hydride Ligands: Reductive Elimination of H_2 and Relevant Thermochemical Fe-H Parameters. *J. Am. Chem. Soc.* **2018**, *140*, 6374–6382.
- (56) Myers, A. L.; Quinn, J. A. Applicability of Henry's Law: An Analysis of the Data of Maharajh and Walkley. *Nature Physical Science* **1972**, 239, 32–32.
- (57) Sylvester, K. T.; Chirik, P. J. Iron-Catalyzed, Hydrogen-Mediated Reductive Cyclization of 1,6-Enynes and Diynes: Evidence for Bis(imino)pyridine Ligand Participation. *J. Am. Chem. Soc.* **2009**, 131. 8772–8774.
- (58) Docherty, J. H.; Peng, J.; Dominey, A. P.; Thomas, S. P. Activation and Discovery of Earth-Abundant Metal Catalysts Using Sodium Tert-Butoxide. *Nat. Chem.* **2017**, *9*, 595–600.